A Methodology for the Indirect Determination and Spatial Resolution of Shear Modulus of PDMS−Silica Elastomers

Brian P. Mayer* and Jeffrey A. Reimer

Department of Chemical Engineering, University of California, Berkeley, Berkeley, California 94720

Robert S. Maxwell

Lawrence Livermore National Laboratory, Livermore, California 94551

Received September 5, 2007; Revised Manuscript Received October 18, 2007

ABSTRACT: A methodology is described that allows for the spatial resolution of shear modulus in silica-filled PDMS elastomers via ^{1}H relaxation measurements and stray-field imaging (STRAFI) techniques. Traditional Hahn echoes provide a simple, robust route to the extraction of a proton residual dipolar coupling constant (RDC), a direct measure of chain mobility and a parameter that can be corollated to numerous mechanical properties. Defining a dimensionless RDC eliminates any artifacts associated with low-field measurement and allows the RDC to become independent of field strength. A direct correlation between the NMR determined dimensionless RDC and results from dynamic mechanical analysis are presented, then employed via STRAFI to determine spatial variations in moduli associated with irradiated elastomeric materials. Reliable performance, despite poorly optimized STRAFI conditions, is demonstrated with an error of no more than 22% between the calculated shear modulus and the measured value via DMA.

1. Introduction

There is considerable need for the development and practical application of methods that can elucidate structural and dynamical changes associated with polymer degradation and aging. For example, the demanding environments to which poly(dimethylsiloxane)-based (PDMS-based) elastomeric materials are exposed often induce subtle microscopic changes of engineering concern resulting in limited device lifetimes. Broadly speaking, experimental methods for the characterization of polymer degradation must be sensitive to changes that occur upon exposure to harsh chemical, physical, mechanical, and radiological environments. Most desirable would be a technique that provides spatial resolution in a noninvasive and nondestructive fashion, yet remains a relatively simple analytical methodology.

Nuclear magnetic resonance spectroscopy (NMR) has been employed for the fundamental studies of polymer-containing materials for over 30 years. Data from these studies show strong correlations between several NMR observables and macroscale polymer properties.[1−8] In the case of elastomeric materials, these properties are dictated to a large degree by network topology. The motional restrictions imposed by chemical cross-links and physical entanglements prevent complete (i.e., isotropic) chain reorientation on the NMR time scale thus partially preserving spatially dependent interactions, in particular the nuclear magnetic dipolar interaction.

More recently, magnetic resonance imaging methods have been employed to provide spatial resolution of residual dipolar interactions through measurement of, for example, transverse (T_2) magnetization decay and multiple quantum coherence buildup.[9,10] In this fashion one can ostensibly map out not only spin density on a pixel-by-pixel basis but also measures of molecular mobility on the order of <1 mm in soft materials.

In this paper we seek to demonstrate the application of residual dipolar couplings (RDCs) toward the imaging of mechanical properties in radiation-damaged silica-filled PDMS elastomers. We determine these couplings for elastomers subjected to various exposures of γ-radiation, correlate them to moduli obtained from dynamic mechanical analysis, and show that moduli can then be imaged using simple MRI methodologies. The correlation between RDC and modulus is scalable down to magnetic fields typically used in portable MR devices, portending the development of standoff ex situ assessment of elastomeric moduli.

2. Experimental Section

The samples studied were a series of poly(dimethylsiloxane)−poly(diphenylsiloxane) silica-filled elastomers exposed to five cumulative doses of up to 50 MRad of γ-irradiation. The pristine sample, unexposed to radiation, was also studied. The details of their preparation and composition can be found elsewhere.[11,12]

^{1}H NMR was conducted at magnetic fields of 0.49, 1.54, and 4.70 T at room temperature under static conditions. The mid-field data were taken with a LapNMR spectrometer (Tecmag, Houston, TX) operating at 65.614 MHz. The low-field data were obtained on a permanent magnet also with a LapNMR spectrometer at 20.7 MHz. Because of the magnet's temperature sensitivity (field shift of approximately 5 kHz/°C), an environmental controller was built to house the magnet and keep the temperature constant within 0.2 °C. High-field work was done on an AMX200 spectrometer (Bruker, Billerica, MA) at 200.13 MHz. All experiments were performed at 25 °C under static conditions, as the highly mobile networks provided significantly narrower proton line widths than those typically seen with polymeric materials, which often exceed 10 kHz. Additionally, as room temperature is significantly above the polymer's glass transition temperature ($T > T_g + 50$ °C), chain mobility will be not dominated by thermal motion but instead only by the topological constraints restricting it (i.e., chemical and physical cross-links and entanglements).

Transverse magnetization decay curves were obtained using the standard Hahn echo, $(\pi/2)_x - \tau - (\pi)_y -$ acquire, combined with CYCLOPS to remove instrumental artifacts. Data were obtained using both commercial and home-built probes, but the $\pi/2$ pulse length was kept around 1.5 μs for all experiments. Because of ^{1}H natural abundance and the probes' relatively high Q values, in general only 12−24 scans were required for exceptional signal-to-noise for a 1−2 mm^3 sample volume. A typical experiment was on the order of 3 h given a repetition delay of 4 s.

* To whom correspondence should be addressed.

10.1021/ma702007m CCC: $40.75
Published on Web 01/19/2008

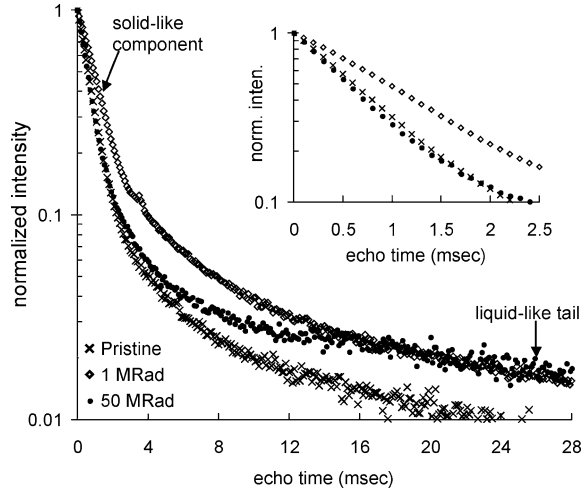

Figure 1. T_2 decay curves for pristine (×), 1 MRad (◇), and 50 MRad (●) samples at 65 MHz. The solidlike decay dominates at short echo times whereas liquidlike populations are seen at times greater than approximately 16 ms. The inset shows the short time decay which is dictated by the motionally-hindered, dipolar-coupled protons.

Images of the samples were acquired using stray-field imaging techniques[13] (STRAFI) at 299.32 MHz with an Apollo console (Tecmag, Houston, TX). The resultant images were one-dimensional and obtained in a constant magnetic field gradient of 0.2 G/cm with little optimization. The strength of the gradient was measured by both glycerol and water diffusion experiments and confirmed by imaging a sample of known length. This relatively low gradient strength was chosen to maintain high signal-to-noise per pixel, as well as demonstrate the technique's validity despite very little additional experimental optimization. The $\pi/2$ pulse length of 10 μs was chosen to ensure relatively uniform excitation across the entire sample height. Spectra were obtained using the Hahn echo method described above. A total of 100 spectra were taken all together which contained each 512 signal averages. With a repetition delay of 4 s, this experiment was 2.5 days in duration.

For all three field strengths used in the relaxation studies, data were analyzed by integrating the magnitude of the FID and baseline correcting in postprocessing. This procedure accounted for any small field drifts of the permanent magnet. Extracted decay curves were normalized to the magnetization after a one-pulse experiment and equivalent experimental conditions (e.g., number of scans, receiver gain, etc.) and fit using nonlinear regression techniques in a standard computational mathematics package. STRAFI images were analyzed in an identical fashion, though the real component of the Fourier transformed, phased spectra was used.

3. Results and Discussion

3.1. Measurement of Proton Residual Dipolar Coupling. As mentioned above, determination of the residual dipolar coupling for this work was done via T_2 decay curves. This method was chosen by virtue of both its experimental and analytical simplicity. Recently, other techniques have been shown to be more accurate, as spin−echo experiments can obfuscate RDC measurement as a result of, for example, dubious model assumptions and fitting ambiguities.[14,15] In general, this group has found, on average, a 30% difference in the couplings measured via T_2 decay and a sine-correlation experiment[16] which filters out all signal but that of dipolar origin (unpublished data). Moreover, since we are presently only concerned with relative changes in the RDC magnitude, we feel that the spin−echo method is adequate.

Figure 1 shows representative transverse magnetization decays for the pristine, 1 and 50 MRad samples at 65 MHz. The solid- and liquidlike decays (due to motionally hindered protons and completely mobile protons, respectively) are temporally separated by virtue of the frequencies of their motions in relation to each other. Rapidly rotating methyl groups contained within liquidlike components are able to sample the entire solid angle, effectively averaging out the dipolar interaction, whereas those of solidlike components only experience a partial averaging of this interaction over the time-scale of the NMR experiment.

Table 1. D_{res} as a Function of Radiation Dosage at 65, 200, and 20 MHz

dose (MRad)	D_{res} (Hz) at 65 MHz	D_{res} (Hz) at 200 MHz	D_{res} (Hz) at 20 MHz
0	260 ± 10	231 ± 10	383 ± 23
1	166 ± 8	159 ± 8	275 ± 18
5	716 ± 4	168 ± 10	260 ± 13
10	178 ± 4	196 ± 15	302 ± 20
25	230 ± 3	225 ± 12	367 ± 19
50	336 ± 3	317 ± 16	519 ± 21

Even though the short-term signal decay determines the RDC magnitude, we have chosen to fit the entire decay envelope since the signal-to-noise ratio is so high (≈100 at short delay times); additionally we were able to obtain the relative contributions to the total decay curve. The data have been fit to an expression for the decay of transverse magnetization, M_x, assuming its applicability to polymer chains subject to topological constraints. $M_x(\tau)$, as a function of echo time, τ, is given by the normalized equation

$$\frac{M_x(\tau)}{M_x(0)} = x_1 \exp[-M_2\tau^2] + \sum_{i=2}^{4} x_i \exp\left[-\frac{\tau}{T_{2,i}}\right] \quad \text{with} \sum_{i=1}^{4} x_i = 1 \quad (1)$$

where x_1 is the relative amount of protons described by M_2, the residual second moment of the dipolar line width and x_i represents one of three transverse relaxation times, $T_{2,i}$. Note that for the first term of eq 1, the factor of $^1/_2$ that appears in strict definitions of the van Vleck second moment has been subsumed into M_2 in the present work. Also, the longest T_2 value corresponds to a small fraction (<5%) of protons associated with freely mobile dangling chain ends, T_2^{de}. T_2^{de} has been fixed at 32.5 ms based on measurements of the unfilled, uncrosslinked gum stock after isolating the liquidlike component (as opposed to relaxation from protons on strongly entangled chains which would exhibit solidlike behavior).

Under the Anderson−Weiss formalism,[17] M_2 (ms^{-2}) is related to the residual dipolar coupling constant, D_{res} (Hz), by the van Vleck second moment:

$$M_2 = \frac{9}{20}\left(\frac{2\pi D_{res}}{1000}\right)^2 \quad (2)$$

Despite identifying several proton environments with different relaxation parameters in accordance with eq 1, reported in the first two columns of Table 1 is solely D_{res} as a function of radiation dose taken at 65 and 200 MHz.

At these two fields, the RDC in general increases over the dosage range, pointing toward reduced motional averaging of the dipolar interaction due to radiation-induced cross-linking of side chains. In contrast, an interesting phenomenon appears at low dosage levels at which a decrease in RDC is observed, implying an increase in segmental mobility. Recent studies have explained this observation in terms of hydrogen bond interruption and a concomitant release of chains at the silica−polymer interface.[11]

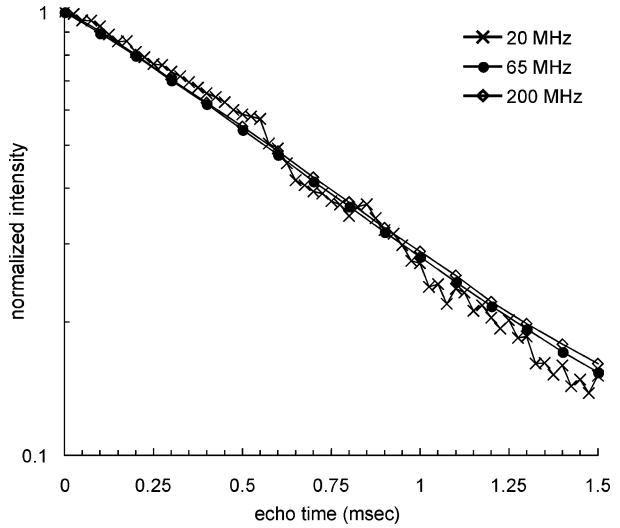

Figure 2. Comparison of initial transverse decay for prisitine sample at 20 MHz (×), 65 MHz (●), and 200 MHz (◊). Discussion of graph found in the text.

In an effort to demonstrate the applicability of this technique at low field, the same data were acquired on a 20 MHz permanent magnet. In principle, the magnitude of the RDC should be independent of the Zeeman field strengh. Previous reports, however, have demonstrated the difficulty in acquiring reliable estimates of RDCs at low fields where field inhomogeneities and susceptibility effects from filler particles can play a large role in obfuscating their measurement.[18] Nevertheless, we have attempted to obtain estimates of the RDCs for the pristine and five irradiated samples.

The last column of Table 1 shows the 20 MHz RDC measured for the samples as compared to the data taken at high field. While a low signal-to-noise ratio (SNR) is not unexpected at 20 MHz, the SNR $\propto \omega_0^{7/4}$ scaling law being well-known, the relatively poor SNR seen here precipitated overestimation of the RDCs by about 50% when compared to data at 65 and 200 MHz. As shown in Figure 2, however, comparison of the initial decay curves out to 1.5 ms (where the component associated with the RDC dominates) shows identical decay patterns suggesting that SNR is affecting RDC extraction to the largest degree as opposed to systematic low-field effects such as microscopic magnetic field gradients at the filler interface (which should have been refocussed to a large extent with the spin−echo sequence). This complication is not unexpected, as the reliability of these measurements depends heavily on not only the model chosen to represent the transverse magnetization decay but also on the quality of the decay data obtained, particularly when the proton component associated with the residual second moment is comparatively small (less than 20% of the total signal).

To compensate for this overestimation, a new dimensionless variable can be created that represents the relative change in RDC as a function of dosage, or in other terms, one that references the RDC at a given dosage, $D_{\text{res}}^{\text{d}}$, to that of the pristine sample, D_{res}^{0}. This quantity, D^*, can be expressed as

$$D^* \equiv \frac{D_{\text{res}}^{\text{d}} - D_{\text{res}}^{0}}{D_{\text{res}}^{0}} \tag{3}$$

whereby, for example, a negative value indicates softening in comparison to the pristine sample. Table 2 and Figure 3 both show this reduced RDC for all dosages and field strengths. For

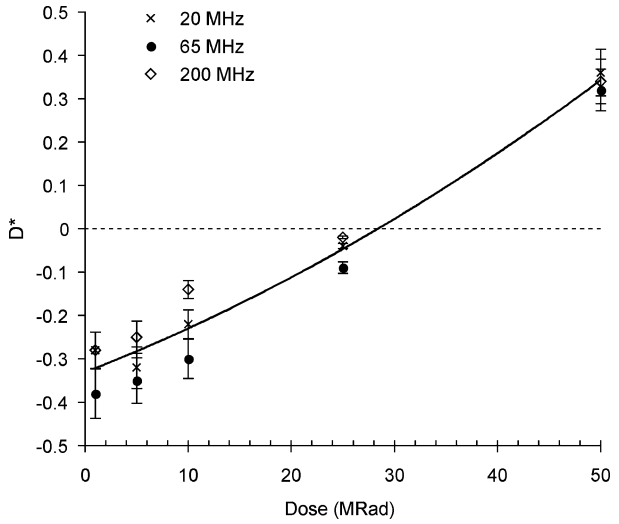

Figure 3. The field-independence of the reduced RDC, D^*, as a function of dosage at 20 MHz (×), 65 MHz (●), and 200 MHz (◊). The bold line is merely a guide for the eye, and the dashed line demarcates the transition from softened to stiffened as compared to the pristine sample.

Table 2. D^* as a Function of Radiation Dosage at All Three Fields, Error Is Estimated at No More than 15%

dose (MRad)	D^* at 20 MHz	D^* at 65 MHz	D^* at 200 MHz
1	−0.28	−0.38	−0.28
5	−0.32	−0.35	−0.25
10	−0.22	−0.30	−0.14
25	−0.04	−0.09	−0.02
50	0.36	0.32	0.34

all fields investigated, D^* is relatively constant for a given radiation dose implying that correlating it to a particular mechanical property is advantageous over its absolute counterpart, as this normalization scheme effectively removes any spurious field dependencies.

3.2. Establishing an NMR/Shear Modulus Correlation. To establish a theoretical link between proton residual dipolar coupling and a macroscopic structural parameter such as shear modulus, we seek to establish a common dependency. The ^{1}H RDC of an isolated, rapidly reorienting methyl group can be expressed as[20]

$$D_{\text{res}}^{(3)} = \frac{\sqrt{6}}{4}(kS^{(3)})\frac{\mathbf{R}^2}{N^2a^2}D^{(3)}P_2(\cos\chi) \tag{4}$$

The rigid dipolar coupling constant, $D^{(3)}$, is defined by $(\mu_0/4\pi)\gamma^2\hbar(1/r^3)$, where r is the distance between methyl protons (0.19 nm). $\mathbf{R}$ is the end-to-end vector of a chain between cross-links, N is the number of statistical segments of length a, and $P_2(\cos\chi)$ is the second-order Legendre polynomial with respect to the angle between the end-to-end vector and the external magnetic field, $\mathbf{B}_0$. The geometric factor k and the order parameter $S^{(3)}$ account for freely jointed chain statistics (for which $k = {}^3/_5$, ref 21) and methyl reorientation of the C_3 axis about $\mathbf{R}$, respectively. An additional factor of $\sqrt{6}/2$ appears when expressing the homonuclear residual dipolar Hamiltonian in terms of the irreducible tensor operator, $T_{2,0}^{(2)}$.[20] Approximating the polymer network as one of the Gaussian disordered chains, a dimensionless end-to-end vector can be defined which is on the order of unity,

$$\mathbf{q}^2 = \frac{\mathbf{R}^2}{\langle\mathbf{R}^2\rangle_{\mathbf{R}}} = \frac{\mathbf{R}^2}{Na^2} \approx 1 \tag{5}$$

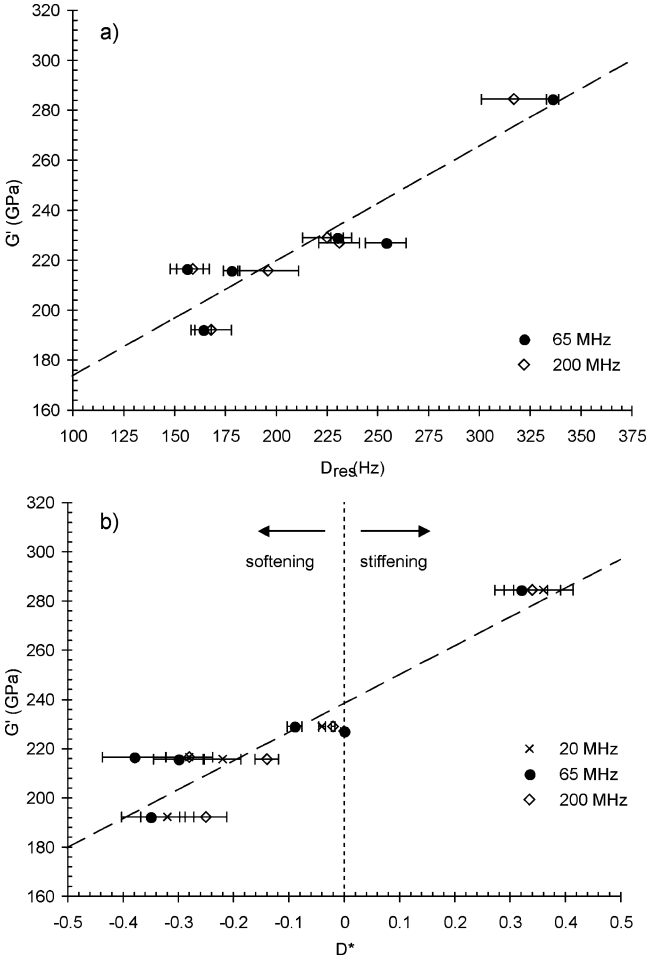

Figure 4. (a) Relation of G' to D_{res} at 65 (●) and 200 MHz (◊). (b) G' versus D^* at all three fields: 20 (×), 65 (●), and 200 MHz (◊). The thick dashed line is the fit according to eq 7. The thin vertical dashed line represents $D^* = 0$, and the arrows indicate the dominant degradation pathway relative to the pristine sample. $R^2 \approx 0.89$.

Table 3. Dynamic Mechanical Analysis: G' as a Function of Dosage[11]

dose (MRad)	G' (GPa)
0	227.0
1	216.6
5	192.2
10	215.8
25	229.0
50	284.5

such that the RDC scales merely as the inverse of the number of chain units, N^{-1}. The storage modulus, G' also scales with the inverse of N through a direct dependence on the cross-link density, υ_c,[22]

$$G' = \upsilon_c k_b T \propto N^{-1} \tag{6}$$

Therefore, assuming the Gaussian assumption holds, there should be a proportional relationship between the residual dipolar coupling and shear modulus. Previous researchers provide data that contradict this assumption. For example, data acquired[11] using dipolar correlation methods[23] do not show this expected proportionality. The lack of proportionality is thought to deviate from Gaussian random chains via mesh chains that are stretched more than expected (presumably due to the nature of the crosslinking in these networks). It is further argued[24] that this deviation from linear behavior may be due to the large-scale cooperative nature of the topological constraints imposed upon the network, which might be thought of as a quasi-nematic potential acting on chain packing. We have nothing further to add to these arguments in the present work, other than to note that the dipolar correlation methods measure coherence loss associated with slower dynamics with time-scales 10^{-4} s $< \tau_c < T_1$, whereas the those associated with the present T_2 decays are 10^{-6} s $< \tau_c < 10^{-3}$ s.

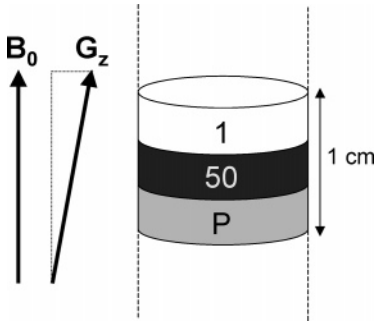

Figure 5. Pictoral representation of elastomer sandwich. Application of the magnetic field gradient, G_z, was assumed to be co-linear with the static magnetic field, $\mathbf{B}_0$, as shown in the diagram. Relative moduli values have been cartooned by shading the slices in various gray tones. Dashed lines indicate 10 mm quartz NMR tube.

Table 3 shows shear modulus data for these samples adapted from Maxwell et al.[11] Figure 4a shows the combination of these data with RDC measurements at both 200 and 65 MHz. Since, however, the absolute RDC data is dependent on the field at which they are measured, we have chosen to establish the modulus/NMR correlation using the dimensionless D^* scheme. Linear regression for these data yield

$$G' = 117[\text{GPa}]D^* + 238[\text{GPa}] \tag{7}$$

The intercept at 238 GPa represents the fit at $D^* = 0$ and an estimation of shear modulus in the absence of irradiation. This corresponds well, within 5%, with the measured value (see Table 3). The relatively high slope of 117 GPa indicates there will be high sensitivity to shear modulus variations for even small changes in the reduced RDC.

With eq 7 there now exists the ability to indirectly determine the modulus, a macroscopic quantity, simply by measuring an NMR parameter that is dictated primarily by polymer chain mobility. An even more useful result, perhaps, is that this correlation is independent of the mechanisms affecting network structure. The data displayed in both graphs of Figure 4 represent the entire irradiation range including both the softening effect that dominates at low dosages and the high-dosage crosslinking. In particular the D^*/G' correlation has shown to be robust to both the magnetic field and various degradation mechanisms.

3.3. Application of the D^*/G' Correlation. For the present work, a sandwich of three samples of different dosages each were made and placed in a 10 mm NMR tube (see Figure 5), and one-dimensional STRAFI images were obtained to test the accuracy of the above correlations in tandem with the imaging modality. The sandwich was constructed to contain modest G' contrast between layers. The direction of the stray field gradient was assumed to be normal to the broad face of the individual sandwich components, but it is important to note that no detailed field mapping was done to determine gradient variation across the sample or any nonlinearities that are likely to be present.

Figure 6 shows a summary of the STRAFI data. Extraction of the residual second moment, M_2, was fairly straightforward, with values comparable to those of the bulk relaxation measurements. The values are larger overall, which is merely an effect of the magnetic field inhomogeneities artificially increasing

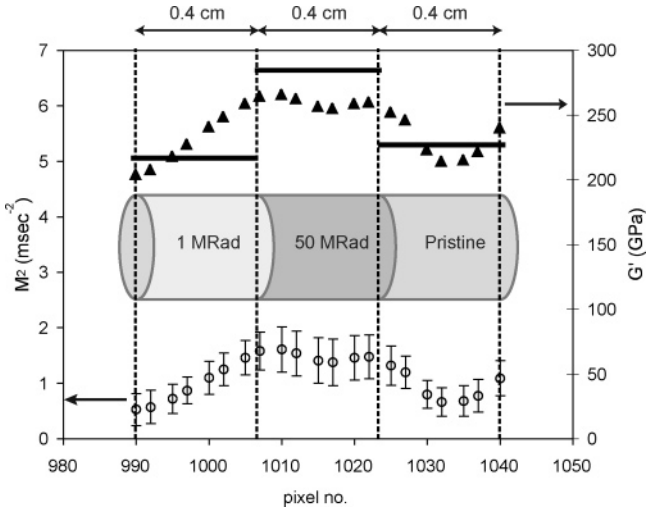

Figure 6. The spatial resolution of residual second moment, M_2, and shear modulus, G'. ○ are pixel-by-pixel M_2 values extracted from the STRAFI data. ▲ are G' calculated from eq 7, and for comparison, the bold lines represent the modulus measured via DMA. The sample sandwich has been underlaid for clarity, and the dashed vertical lines indicate boundaries of the individual sandwich components. Sample size has also been indicated above the graph. Total height of sample is 1.2 cm.

relaxation rates. Employing the methodology outlined above, we convert M_2 to D_{res} and D_{res} to D^* via eqs 2 and 3, respectively. Use of eq 7 yields the calculated G' values shown in the figure. As indicated in the caption, the bold line represents the modulus as measured by DMA. The lack of a clear break in the M_2 and calculated G' values at the sample interfaces (pixels 1006 and 1023) results from the low gradient strength, as the frequency spread for a given pixel barely overcomes the natural proton line width. This fact explains the apparent continuum of values seen across the sandwich height; there is, in effect, a bleed-through of information between pixels. Moreover, there is no need to know the gradient strength or nonlinearities across the sample, as the correlation does not require this type of information. Despite these potentially serious pitfalls, the error between the correlated and measured (i.e., NMR vs DMA) values is at most 20% which we take to be acceptable considering this lack of optimization usually present in STRAFI experiments.

As this methodology is clearly independent of the imaging modality, one could quite easily extend it to multiple dimensions, acquiring a fully three-dimensional data set. Using pulsed field-gradient imaging techniques would certainly only enhance the data quality, as the experimentalist would have full control over gradient strength and linearity and would be able to suppress artifacts due to natural line width bleed-through. One minor complication, that being the acquisition of images at short delay times, could be easily compensated for by the use of SPRITE techniques developed to address just this issue.[25]

4. Conclusions

The present work has demonstrated the utility of transverse magnetization decay in the extraction of proton residual dipolar coupling constants and their subsequent imaging. Despite recent criticism of various T_2 methods, we have demonstrated the present methodology to be more than adequate since we are presently only concerned with relative changes in the RDC magnitude, as opposed to their absolute counterparts. These data were used in conjunction with dynamic mechanic analysis to establish a correlation between a measure of chain mobility and the bulk shear modulus of PDMS−silica elastomers. A field-independent, reduced RDC was defined that opened up the possibility of low-field measurement, making this technique particularly attractive, as inexpensive permanent magnets and portable single-sided systems are more amenable to efficient, in-field diagnostics.

We also recognize that various exact decay expressions have been developed (including some from our own laboratory) which rely purely on polymer statistical theories and not on the second moment approximation exploited above. Research is currently being conducted using these expressions that will be used in conjunction with the present samples in part for a truly model-free determination of shear modulus via NMR.

Acknowledgment. Mr. Mayer would like to thank S. Chinn and J. Herberg (of LLNL) for helpful discussions and assistance on Livermore equipment. This work was performed under the auspices of the U.S. Department of Energy by the Lawrence Livermore National Laboratory under Contract No. W-7405-ENG-48. Part of this work was also supported by the LLNL Laboratory Directed Research and Development (LDRD) program (tracking number: 06-SI-005).

References and Notes

(1) Marcinko, J. J.; Parker, A. A.; Shieh, Y. T.; Ritchey, W. M. *J. Appl. Polym. Sci.* **1992**, *45*, 391−398.
(2) Parker, A. A.; Marcinko, J. J.; Rinaldi, P.; Hedrick, D. P.; Ritchey, W. M. *J. Appl. Polym. Sci.* **1993**, *48*, 677−681.
(3) Fischer, E.; Grinberg, F.; Kimmich, R.; Hafner, S. *J. Chem. Phys.* **1998**, *109*, 846−854.
(4) Litvinov, V. M.; Dias, A. A. *Macromolecules* **2001**, *34*, 4051−4060.
(5) Fechete, R.; Demco, D. E.; Blümich, B. *J. Chem. Phys.* **2003**, *118*, 2411−2421.
(6) Maus, A.; Hertlein, C.; Saalwächter, K. *Macromol. Chem. Phys.* **2006**, *207*, 1150−1158.
(7) Saalwächter, K.; Gottlieb, M.; Lie, R. G.; Oppermann, W. *Macromolecules* **2007**, *40*, 1555−1561.
(8) Ries, M. E.; Brereton, M. G.; Klein, P. G.; Ward, I. M.; Ekanayake, P.; Menge, H.; Schneider, R. *Macromolecules* **1999**, *32*, 4961−4968.
(9) Klinkenberg, M.; Blümler, P.; Blümich, B. *Macromolecules* **1997**, *30*, 1038−1043.
(10) Fechete, R.; Demco, D. E.; Blümich, B. *J. Magn. Reson.* **2003**, *165*, 9−17.
(11) Maxwell, R. S.; Balazs, B. *J. Chem. Phys.* **2002**, *116*, 10492−10502.
(12) Chien, A.; Maxwell, R. S.; Chambers, D.; Balazs, B.; LeMay, J. *Rad. Phys. Chem.* **2000**, *59*, 493−500.
(13) McDonald, P. J.; Newling, B. *Rep. Prog. Phys.* **1998**, *61*, 1441−1493.
(14) Whittaker, A. K.; Bremner, T.; Zelaya, F. O. *Polymer* **1995**, *36*, 2159−2164.
(15) Saalwächter, K. *Prog. Nucl. Magn. Reson. Spectrosc.* **2007**, *51*, 1−35.
(16) Callaghan, P. T.; Samulski, E. T. *Macromolecules* **1997**, *30*, 113−122.
(17) Anderson, P. W.; Weiss, P. R. *Rev. Mod. Phys.* **1953**, *25*, 269−276.
(18) Saalwächter, K. *Macromolecules* **2005**, *38*, 1508−1512.
(19) Sotta, P.; Deloche, B. *Macromolecules* **1990**, *23*, 1999−2007.
(20) Schneider, M.; Gasper, L.; Demco, D. E.; Blümich, B. *J. Chem. Phys.* **1999**, *111*, 402−415.
(21) Treloar, L. R. G. *Trans. Faraday Soc.* **1954**, *50*, 881−896.
(22) Jenkins, R. K. *J. Polym. Sci.* **1966**, *4*, 41−52.
(23) Fischer, E.; Grinberg, F.; Kimmich, R.; Hafner, S. *J. Chem. Phys.* **1998**, *109*, 846−854.
(24) Saalwächter, K.; Sommer, J. U. *Macromol. Rapid Commun.* **2007**, *28*, 1455−1465.
(25) Kennedy, C. B.; Balcom, B. J.; Kastikhin, I. V. *Can. J. Chem.* **1998**, *76*, 1753−1765.

MA702007M